PHYSICAL REVIEW D **87,** 114013 (2013)

Exclusive diffractive photon bremsstrahlung at the LHC

Piotr Lebiedowicz[1,*] and Antoni Szczurek[1,2,†]
[1]*Institute of Nuclear Physics PAN, PL-31-342 Cracow, Poland*
[2]*University of Rzeszów, PL-35-959 Rzeszów, Poland*
(Received 12 March 2013; published 14 June 2013)

We calculate differential distributions for the $pp \to pp\gamma$ reaction at the LHC energy $\sqrt{s} = 14$ TeV. We consider diffractive classical bremsstrahlung mechanisms including effects of the non-point-like nature of protons. In addition, we take into account (vector meson)-pomeron, photon-pion, and photon-pomeron exchange processes for the first time in the literature. Predictions for the total cross section and several observables related to these processes, e.g., differential distributions in pseudorapidities and transverse momenta of photons or protons are shown and discussed. The integrated diffractive bremsstrahlung cross section ($E_\gamma > 100$ GeV) is only of the order of μb. We try to identify regions of the phase space where one of the mechanisms dominates. The classical bremsstrahlung dominates at large forward/backward photon pseudorapidities, close to the pseudorapidities of scattered protons. In contrast, the photon-pomeron (pomeron-photon) mechanism dominates at midrapidities but the related cross section is rather small. In comparison the virtual-omega–rescattering mechanism contributes at smaller angles of photons (larger photon rapidities). Photons in the forward/backward region can be measured by the Zero Degree Calorimeters installed in experiments at the LHC while the midrapidity photons are difficult to measure (small cross section, small photon transverse momenta). Protons could be measured by the ALFA detector (ATLAS) or TOTEM detector at CMS. The exclusivity could be checked with the help of main central detectors.

DOI: 10.1103/PhysRevD.87.114013 PACS numbers: 13.60.Le, 12.40.Nn, 13.85.−t, 14.40.Be

I. INTRODUCTION

An exclusive diffractive photon bremsstrahlung mechanism at high energies has almost never been studied in the literature. Because at high energy the pomeron exchange is the driving mechanism of bremsstrahlung it is logical to call the mechanisms described by the diagrams shown in Fig. 1 diffractive bremsstrahlung to distinguish them from the low-energy bremsstrahlung driven by meson exchanges.[1] The exclusive photon production mechanism is similar to the $pp \to pp\omega$ [3] and $pp \to pp\pi^0$ [4] processes. As discussed in the past the dominant hadronic bremsstrahlung-type mechanism is the Drell-Hiida-Deck mechanism [5] for the diffractive production of πN final states (for a nice review we refer to Ref. [6] and references therein).

The $pp \to pp\gamma$ process at high energies was discussed only recently [7] and it was proposed to use the exclusive photon bremsstrahlung to measure or estimate the elastic proton-proton cross section at the LHC. Only approximate formulas for the classical bremsstrahlung were given there. The participating particles were treated there as point-like particles. No differential distributions for the exclusive bremsstrahlung have been discussed.

The photons radiated off the initial- and final-state protons can be seen by the Zero Degree Calorimeters (ZDCs) that are installed at about 140 meters on each side of the interaction region. They will measure very forward neutral particles in the pseudorapidity region $|\eta| > 8.5$ at the CMS [8] and the ATLAS ZDCs provide coverage of the region $|\eta| > 8.3$ [9].[2] The forward detectors beyond pseudorapidities of $|\eta| > 3$ provide an efficient veto against neutral particle backgrounds in the ZDCs from diffractive and nondiffractive events (see Ref. [7]). Furthermore the proposed Forward Shower Counters, to detect and trigger on rapidity gaps in diffractive events, would improve the measurements at the LHC significantly [11]. In addition to a measurement of the elastic pp cross section the bremsstrahlung photons could allow for the evaluation of the total pp cross section, luminosity, and relative alignment of the ZDCs and of the Roman Pot detectors.

In this paper, we wish to present the first detailed study of single-photon bremsstrahlung in the exclusive process $pp \to pp\gamma$ at the LHC energy $\sqrt{s} = 14$ TeV. We shall include classical bremsstrahlung diagrams as well as some

---

[*] Piotr.Lebiedowicz@ifj.edu.pl
[†] Antoni.Szczurek@ifj.edu.pl

[1] The photon bremsstrahlung was intensively studied in nucleon-nucleon collisions at low energies (see, e.g., Refs. [1,2] and references therein). There the dominant mechanisms are nucleon-current (off-shell nucleon) and/or mesonic-current (photon emitted from the middle of exchanged mesons) contributions driven by meson exchanges.

[2] Recently, the exclusive $pp \to nn\pi^+\pi^+$ reaction has been studied in Ref. [10]. This reaction can also be measured with the help of the ZDC detectors. Very large cross sections have been found, which are partially due to the interference of a few mechanisms. The presence of several interfering mechanisms precludes the extraction of the elastic $\pi^+\pi^+$ scattering cross section.

© 2013 American Physical Society

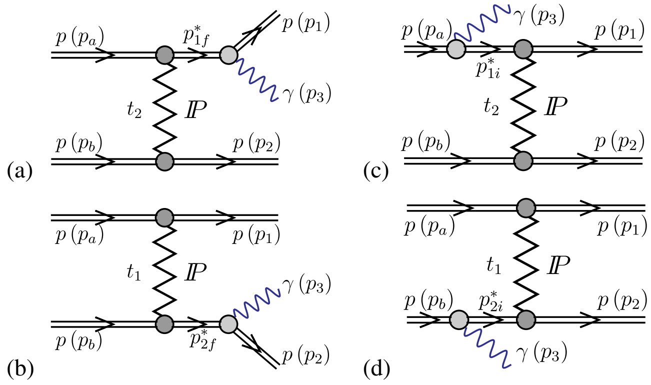

FIG. 1 (color online). Diagrams of the bremsstrahlung amplitudes driven by the pomeron exchange.

new diagrams that are exclusively characteristic for proton-proton scattering, which are not present, e.g., in e^+e^- scattering. We include diagrams which arise in the vector-dominance model as well as photon-pion (pion-photon) and photon-pomeron (pomeron-photon) exchange processes not discussed so far in the literature. We shall try to identify the region of the phase space where one can expect a dominance of one of the processes through detailed studies of several differential distributions.

II. THE AMPLITUDES FOR THE $pp \to pp\gamma$ REACTION

A. Diffractive classical bremsstrahlung mechanisms

The bremsstrahlung mechanisms for the exclusive production of photons discussed here are shown schematically in Fig. 1. In the case of γ production the diagrams with intermediate nucleon resonances (see Ref. [12]) should be negligible. The proton to Δ isobar transitions pronounced at low energy are suppressed in the high-energy regime.

The Born amplitudes of the diagrams shown in Fig. 1 can be written as

$$\begin{aligned}\mathcal{M}^{(a)}_{\lambda_a\lambda_b\to\lambda_1\lambda_2\lambda_3} = {}& e\bar{u}(p_1,\lambda_1)\not{\varepsilon}^*(p_3,\lambda_3)S_N(p_{1f}^2)\gamma^\mu u(p_a,\lambda_a)\\ &\times F_{\gamma N^*N}(p_{1f}^2)F_{\mathbb{P}NN^*}(p_{1f}^2)\\ &\times isC_{\mathbb{P}}^{NN}\left(\frac{s}{s_0}\right)^{\alpha_{\mathbb{P}}(t_2)-1}\exp\left(\frac{B_{\mathbb{P}}^{NN}t_2}{2}\right)\\ &\times\frac{1}{2s}\bar{u}(p_2,\lambda_2)\gamma_\mu u(p_b,\lambda_b), \qquad (2.1)\end{aligned}$$

$$\begin{aligned}\mathcal{M}^{(b)}_{\lambda_a\lambda_b\to\lambda_1\lambda_2\lambda_3} = {}& e\bar{u}(p_2,\lambda_2)\not{\varepsilon}^*(p_3,\lambda_3)S_N(p_{2f}^2)\gamma^\mu u(p_b,\lambda_b)\\ &\times F_{\gamma N^*N}(p_{2f}^2)F_{\mathbb{P}NN^*}(p_{2f}^2)\\ &\times isC_{\mathbb{P}}^{NN}\left(\frac{s}{s_0}\right)^{\alpha_{\mathbb{P}}(t_1)-1}\exp\left(\frac{B_{\mathbb{P}}^{NN}t_1}{2}\right)\\ &\times\frac{1}{2s}\bar{u}(p_1,\lambda_1)\gamma_\mu u(p_a,\lambda_a), \qquad (2.2)\end{aligned}$$

$$\begin{aligned}\mathcal{M}^{(c)}_{\lambda_a\lambda_b\to\lambda_1\lambda_2\lambda_3} = {}& e\bar{u}(p_1,\lambda_1)\gamma^\mu S_N(p_{1i}^2)\not{\varepsilon}^*(p_3,\lambda_3)u(p_a,\lambda_a)\\ &\times F_{\gamma NN^*}(p_{1i}^2)F_{\mathbb{P}N^*N}(p_{1i}^2)\\ &\times is_{12}C_{\mathbb{P}}^{NN}\left(\frac{s_{12}}{s_0}\right)^{\alpha_{\mathbb{P}}(t_2)-1}\exp\left(\frac{B_{\mathbb{P}}^{NN}t_2}{2}\right)\\ &\times\frac{1}{2s_{12}}\bar{u}(p_2,\lambda_2)\gamma_\mu u(p_b,\lambda_b), \qquad (2.3)\end{aligned}$$

$$\begin{aligned}\mathcal{M}^{(d)}_{\lambda_a\lambda_b\to\lambda_1\lambda_2\lambda_3} = {}& e\bar{u}(p_2,\lambda_2)\gamma^\mu S_N(p_{2i}^2)\not{\varepsilon}^*(p_3,\lambda_3)u(p_b,\lambda_b)\\ &\times F_{\gamma NN^*}(p_{2i}^2)F_{\mathbb{P}N^*N}(p_{2i}^2)\\ &\times is_{12}C_{\mathbb{P}}^{NN}\left(\frac{s_{12}}{s_0}\right)^{\alpha_{\mathbb{P}}(t_1)-1}\exp\left(\frac{B_{\mathbb{P}}^{NN}t_1}{2}\right)\\ &\times\frac{1}{2s_{12}}\bar{u}(p_1,\lambda_1)\gamma_\mu u(p_a,\lambda_a), \qquad (2.4)\end{aligned}$$

where $u(p,\lambda)$, $\bar{u}(p',\lambda') = u^\dagger(p',\lambda')\gamma^0$ are the Dirac spinors [normalized as $\bar{u}(p')u(p) = 2m_p$] of the initial and outgoing protons with the four-momentum p and the helicities λ. The factor $\frac{1}{2s}$ or $\frac{1}{2s_{12}}$ appear here as a consequence of using spinors. The four-momenta squared of virtual nucleons in the middle of the diagrams are defined as $t_{1,2} = q_{1,2}^2 = (p_{a,b} - p_{1,2})^2$, $p_{1i,2i}^2 = (p_{a,b} - p_3)^2$, and $p_{1f,2f}^2 = (p_{1,2} + p_3)^2$, and $s_{ij} = W_{ij}^2 = (p_i + p_j)^2$ are squared invariant masses of the (i,j) system. The propagators of the intermediate nucleons can be written as

$$S_N(p^2) = \frac{i(\not{p} + m_p)}{p^2 - m_p^2}, \qquad (2.5)$$

where $\not{p} = p_\mu\gamma^\mu$. The polarization vectors of the real photon [$\not{\varepsilon}^*(p_3,\lambda_3) = \gamma^\nu\varepsilon_\nu^*(p_3,\lambda_3)$] are defined in the proton-proton center-of-mass frame,

$$\begin{aligned}\varepsilon_\nu(p_3,\pm1) = {}& \frac{1}{\sqrt{2}}(0, i\sin\phi \mp \cos\theta\cos\phi,\\ & -i\cos\phi \mp \cos\theta\sin\phi, \pm\sin\theta), \qquad (2.6)\end{aligned}$$

where θ is the polar angle and ϕ is the azimuthal angle of an emitted photon. It is easy to check that they fulfill the relations $\varepsilon^\nu(p,\lambda)\varepsilon_\nu^*(p,\lambda) = -1$ and $p^\nu\varepsilon_\nu(p,\lambda) = 0$.

We use the interaction parameters of Donnachie-Landshoff [13] with $C_{\mathbb{P}}^{NN} = 21.7$ mb and the pomeron trajectory $\alpha_{\mathbb{P}}(t)$ linear in t,

$$\begin{aligned}\alpha_{\mathbb{P}}(t) = \alpha_{\mathbb{P}}(0) + \alpha'_{\mathbb{P}}t, \qquad & \alpha_{\mathbb{P}}(0) = 1.0808,\\ \alpha'_{\mathbb{P}} = 0.25\ \mathrm{GeV}^{-2}. & \qquad (2.7)\end{aligned}$$

The pomeron slope can be written as

$$B(s) = B_{\mathbb{P}}^{NN} + 2\alpha'_{\mathbb{P}}\ln\left(\frac{s}{s_0}\right), \qquad (2.8)$$

where we use $s_0 = 1\ \mathrm{GeV}^2$ and $B_{\mathbb{P}}^{NN} = 9\ \mathrm{GeV}^{-2}$, which approximately describes a running slope for proton-proton elastic scattering. Since in our calculations we include effective pomerons, i.e., pomerons describing approximately nucleon-nucleon elastic scattering, no explicit absorption corrections have to be included in the addition.

In the bremsstrahlung processes discussed here the intermediate nucleons are off-mass shell. In our approach the off-shell effects related to the non-point-like protons in the intermediate state are included by the following simple extra form factors:

$$F(p^2) = \frac{\Lambda_N^4}{(p^2 - m_p^2)^2 + \Lambda_N^4}. \tag{2.9}$$

This form was used, e.g., in Ref. [14] for ω photoproduction. In general, the cutoff parameters in the form factors are not known but could be fitted in the future to the (normalized) experimental data. From our general experience in hadronic physics we expect $\Lambda_N \sim 1$ GeV. We shall discuss how the uncertainties of the form factors influence our final results.

We could "improve" the parametrization of the amplitudes (2.3) and (2.4) to reproduce the high-energy Regge dependence by the factors $(s_{13}/m_p^2)^{\alpha_N(p_{1i}^2)-\frac{1}{2}}$ and $(s_{23}/m_p^2)^{\alpha_N(p_{2i}^2)-\frac{1}{2}}$, respectively, where the nucleon trajectory is $\alpha_N(p_{1i,2i}^2) = -0.3 + \alpha_N' p_{1i,2i}^2$, with $\alpha_N' = 0.9\ \mathrm{GeV}^{-2}$. We leave the problem of consistent nucleon Reggezation in the context of high-energy photon bremsstrahlung for future studies.

In the present paper we consider a so-called vector model of the pomeron, sometimes called the Donnachie-Landshoff model. This model is known to have some deficiencies. For example, in Ref. [15] it was shown that this model when applied to quark-antiquark production in deep inelastic scattering violates gauge invariance. The main problems there are for virtual photons and for the coupling of the pomeron to the quark and antiquark. In the present paper we consider real photons and coupling to protons. The coupling of anything to extended, off-shell objects, like nucleons, requires special care. This is especially true when electromagnetic interactions come into play (see, e.g., Ref. [16]). The introduction of form factors for extended objects is one of potential sources of gauge-invariance violation, which can be easily checked for an academic case when the effective pomeron exchange is replaced by t-channel photon exchange. There are no general and systematic methods of how to treat this problem. In general, in effective theories contact terms appear. The simple pomeron model considered here is certainly not the final word in the field. Furthermore there are good arguments that the tensor pomeron could be an alternative [17–19]. Further studies are necessary to find an optimal model for the effective pomeron exchange and how the form factors for off-shell non-point-like particles should be constructed to preserve gauge invariance.

B. Bremsstrahlung of ω mesons

In Ref. [3] we have discussed bremsstrahlung of ω mesons. There one includes processes when a ω meson emitted by an (anti)proton interacts with the second (anti) proton. The Born amplitudes for the interaction with the emitted virtual ω meson and its subsequent transformation to a photon, shown in Fig. 2, are obtained as

$$\begin{aligned}\mathcal{M}^{(e)\omega\mathbb{P}-\mathrm{exch}}_{\lambda_a\lambda_b\to\lambda_1\lambda_2\lambda_3} &= \bar{u}(p_1,\lambda_1)\gamma^\mu u(p_a,\lambda_a) S_{\mu\nu}(t_1)\varepsilon^{\nu *}(p_3,\lambda_3)\\ &\quad\times g_{\omega NN} F_{\omega^* NN}(t_1) F_{\mathbb{P}\omega^*\omega}(t_1)\\ &\quad\times C_{\omega\to\gamma}\, i s_{23} C_{\mathbb{P}}^{\omega N}\left(\frac{s_{23}}{s_0}\right)^{\alpha_{\mathbb{P}}(t_2)-1}\left(\frac{s_{13}}{s_{\mathrm{thr}}}\right)^{\alpha_\omega(t_1)-1}\\ &\quad\times\exp\left(\frac{B_{\mathbb{P}}^{\omega N} t_2}{2}\right)\delta_{\lambda_2\lambda_b},\end{aligned} \tag{2.10}$$

$$\begin{aligned}\mathcal{M}^{(f)\mathbb{P}\omega-\mathrm{exch}}_{\lambda_a\lambda_b\to\lambda_1\lambda_2\lambda_3} &= \bar{u}(p_2,\lambda_2)\gamma^\mu u(p_b,\lambda_b) S_{\mu\nu}(t_2)\varepsilon^{\nu *}(p_3,\lambda_3)\\ &\quad\times g_{\omega NN} F_{\omega^* NN}(t_2) F_{\mathbb{P}\omega^*\omega}(t_2)\\ &\quad\times C_{\omega\to\gamma}\, i s_{13} C_{\mathbb{P}}^{\omega N}\left(\frac{s_{13}}{s_0}\right)^{\alpha_{\mathbb{P}}(t_1)-1}\left(\frac{s_{23}}{s_{\mathrm{thr}}}\right)^{\alpha_\omega(t_2)-1}\\ &\quad\times\exp\left(\frac{B_{\mathbb{P}}^{\omega N} t_1}{2}\right)\delta_{\lambda_1\lambda_a},\end{aligned} \tag{2.11}$$

where $S_{\mu\nu}(t)$ is the propagator of the ω meson,

$$S_{\mu\nu}(t) = \frac{-g_{\mu\nu} + \frac{q_\mu q_\nu}{m_\omega^2}}{t - m_\omega^2}. \tag{2.12}$$

In our calculation we assume $C_{\mathbb{P}}^{\omega N} = C_{\mathbb{P}}^{\pi N} = 13.63$ mb [13] and the slope parameter $B_{\mathbb{P}}^{\omega N} = B_{\mathbb{P}}^{\pi N} = 5.5\ \mathrm{GeV}^{-2}$ (see, e.g., Refs. [3,20]). The amplitudes above, Eqs. (2.10) and (2.11), are corrected to reproduce the high-energy Regge dependence by the Regge-like factors $(s_{13}/s_{\mathrm{thr}})^{\alpha_\omega(t_1)-1}$ and $(s_{23}/s_{\mathrm{thr}})^{\alpha_\omega(t_2)-1}$, respectively. The ω-Reggeon trajectory is taken as $\alpha_\omega(t) = 0.5 + 0.9t$ and $s_{\mathrm{thr}} = (m_p + m_\omega)^2$.

Different values of the omega meson to nucleon coupling constant have been used in the literature [21]. In our calculation we assume a coupling constant $g_{\omega NN}^2/4\pi = 10$. A similar value was used in Refs. [22,23]. The transformation of the ω meson to a photon is obtained within the vector dominance model [24] and $C_{\omega\to\gamma} = \sqrt{\alpha_{\mathrm{em}}/20.5} \simeq 0.02$, $\alpha_{\mathrm{em}} = e^2/(4\pi)$.

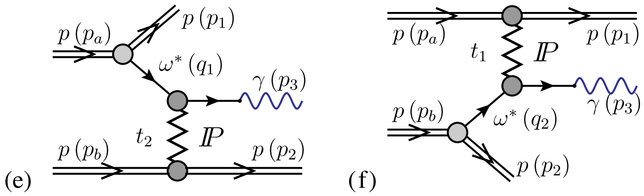

FIG. 2 (color online). Diagrams of the bremsstrahlung amplitudes with the virtual ω meson (Reggeon) and its transformation to a final-state photon.

For the completeness of this analysis we should also include amplitudes for the interaction with the emitted (virtual) ρ meson. Because of isospin, there is no mixing between the intermediate ω and ρ mesons. The transition of the ρ meson to a photon is more probable, $C_{\rho\to\gamma} = \sqrt{\alpha_{\rm em}/2.54} \simeq 0.05$, whereas the coupling constant $g_{\rho NN}$ is small compared with $g_{\omega NN}$; as a consequence the $\rho - \mathbb{P}$ contribution is comparable to the $\omega - \mathbb{P}$ contribution.

The off-shell form factors $F_{\omega^* NN}$ and $F_{\mathbb{P}\omega^*\omega}$ in Eqs. (2.10) and (2.11) will be taken here in the following exponential form:

$$F_{\omega^* NN}(t) = \exp\left(\frac{t - m_\omega^2}{\Lambda_{\omega NN}^2}\right), \qquad F_{\mathbb{P}\omega^*\omega}(t) = \exp\left(\frac{t - m_\omega^2}{\Lambda_{\mathbb{P}\omega\omega}^2}\right), \tag{2.13}$$

where $\Lambda_{\omega NN} = \Lambda_{\mathbb{P}\omega\omega} = 1$ GeV.

C. Pion cloud ($\gamma\pi^0$ and $\pi^0\gamma$ exchanges)

In our present analysis we also include $\gamma\pi^0$ and $\pi^0\gamma$ exchanges. The underlying mechanisms are shown in Fig. 3. Such diagrams are dictated by the presence of a pion cloud in the nucleon (see, e.g., Ref. [25]).

The amplitudes for the two new processes can be easily written as

$$\begin{aligned}\mathcal{M}^{(g)\gamma\pi^0-\text{exch}}_{\lambda_a\lambda_b\to\lambda_1\lambda_2\lambda_3} &= e\bar{u}(p_1,\lambda_1)\gamma^\alpha u(p_a,\lambda_a)F_1(t_1)\frac{-g_{\alpha\beta}}{t_1}\\ &\quad\times F_{\gamma\pi\to\gamma}(t_1,t_2)\varepsilon^{\beta\mu\nu\lambda}q_{1\mu}p_{3\nu}\varepsilon^*_\lambda(p_3,\lambda_3)\\ &\quad\times g_{\pi^0 NN}F_{\pi NN}(t_2)\frac{1}{t_2 - m_\pi^2}\bar{u}(p_2,\lambda_2)\\ &\quad\times i\gamma_5 u(p_b,\lambda_b),\end{aligned} \tag{2.14}$$

$$\begin{aligned}\mathcal{M}^{(h)\pi^0\gamma-\text{exch}}_{\lambda_a\lambda_b\to\lambda_1\lambda_2\lambda_3} &= g_{\pi^0 NN}F_{\pi NN}(t_1)\frac{1}{t_1 - m_\pi^2}\bar{u}(p_1,\lambda_1)\\ &\quad\times i\gamma_5 u(p_a,\lambda_a)\frac{-g_{\alpha\beta}}{t_2}F_{\gamma\pi\to\gamma}(t_2,t_1)\\ &\quad\times \varepsilon^{\beta\mu\nu\lambda}q_{2\mu}p_{3\nu}\varepsilon^*_\lambda(p_3,\lambda_3)e\bar{u}(p_2,\lambda_2)\\ &\quad\times \gamma^\alpha u(p_b,\lambda_b)F_1(t_2),\end{aligned} \tag{2.15}$$

where the $\gamma^* NN$ vertices are parametrized by the proton Dirac electromagnetic form factors,

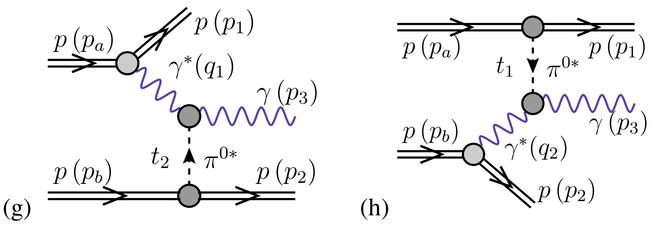

FIG. 3 (color online). Diagrams with the $\gamma\pi^0$ and $\pi^0\gamma$ exchanges in the $pp \to pp\gamma$ reaction.

$$F_1(t) = \frac{4m_p^2 - 2.79t}{(4m_p^2 - t)(1 - t/m_D^2)^2}, \tag{2.16}$$

where m_p is the proton mass and $m_D^2 = 0.71$ GeV^2. The coupling of the pion to the nucleon, $g_{\pi NN}^2/4\pi = 13.5$, is relatively well known (see, e.g., Ref. [26]), and the corresponding hadronic form factor is taken in the exponential form,

$$F_{\pi NN}(t) = \exp\left(\frac{t - m_\pi^2}{\Lambda_{\pi NN}^2}\right), \tag{2.17}$$

with $\Lambda_{\pi NN} = 1$ GeV. For the central vertices involving off-shell particles the $\gamma\pi^0$ form factors are taken in the following factorized form:

$$F_{\gamma\pi\to\gamma}(t_1,t_2) = \frac{N_c}{12\pi^2 f_\pi}\frac{m_\rho^2}{m_\rho^2 - t_1}\exp\left(\frac{t_2 - m_\pi^2}{\Lambda_{\gamma\pi\to\gamma}^2}\right), \tag{2.18}$$

with the pion decay constant $f_\pi = 93$ MeV and $N_c = 3$. The factor describing the virtual photon coupling is taken as in the vector dominance model. In practical calculations we take $\Lambda_{\gamma\pi\to\gamma} = 1$ GeV.

D. Photon rescattering (γIP and $IP\gamma$ exchanges)

At high energy there is still another type of diagram (mechanism) shown in Fig. 4. In the following diagrams we shall call them i) and j) for simplicity. Here the intermediate photon couples to one of the protons through electromagnetic form factors and interacts (at high energies) with the second proton-exchanging pomeron (phenomenology) or gluonic ladder in the QCD language (see, e.g., Ref. [27]). This is a counterpart of the diagrams g) and h) (see Fig. 3), which are relevant at lower γp subenergies.

The amplitude of the three-body process can be written in terms of the amplitude for elastic γp scattering. For not too large t the $\gamma p \to \gamma p$ amplitude can be simply parametrized as

$$\mathcal{M}_{\gamma p\to\gamma p}(s,t) \cong is\sigma_{\rm tot}^{\gamma p}(s)\exp\left(\frac{B_{\gamma p}}{2}t\right). \tag{2.19}$$

Such an amplitude gives, however, the correct total cross section by construction. In the calculations presented in the Results section we shall use the simple Donnachie-Landshoff fit to the world data on the photon-proton total cross section [13] in which the pomeron and subleading Reggeon exchanges[3] have been included,

$$\begin{aligned}\sigma_{\rm tot}^{\gamma p}(s) &= C_{\mathbb{P}}^{\gamma p}s^{\alpha_{\mathbb{P}}(0)-1} + C_{\mathbb{R}}^{\gamma p}s^{\alpha_{\mathbb{R}}(0)-1}, \quad C_{\mathbb{P}}^{\gamma p} = 0.0677\ \text{mb},\\ C_{\mathbb{R}}^{\gamma p} &= 0.129\ \text{mb}, \quad \alpha_{\mathbb{P}}(0) = 1.0808, \quad \alpha_{\mathbb{R}}(0) = 0.5475.\end{aligned} \tag{2.20}$$

---

[3] In the Reggeon contribution the f_2 exchange dominates over the a_2 exchange similarly to the hadronic reactions; see, e.g., Ref. [28].

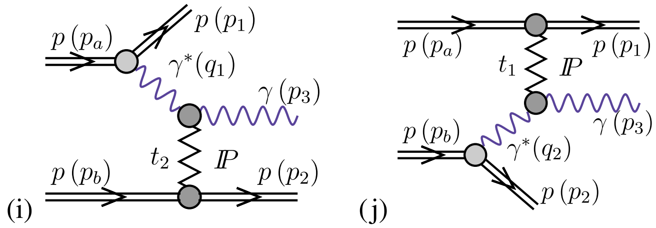

FIG. 4 (color online). Diagrams with the $\gamma\mathbb{P}$ and $\mathbb{P}\gamma$ exchanges for the $pp \to pp\gamma$ reaction.

In general, the slope parameter could be found by fitting to elastic γp scattering data which are, however, unknown and very difficult to measure. Since the incoming photon must first fluctuate to the $q\bar{q}$ state which interacts by the pomeron exchange with a proton before forming the outgoing vector meson, it seems reasonable to use a hadronic slope for a first estimation. In practical calculations we shall use $B_{\gamma p}(s) = B_{\pi p}(s)$ with its energy dependence; see Eq. (2.8).

Having fixed the elementary $\gamma p \to \gamma p$ amplitude we can proceed to our three-body photon rescattering amplitude. Limiting to large energies and small transverse momenta t_1 and t_2, for helicity conserving processes the matrix element can be written as

$$\begin{aligned}\mathcal{M}_{\lambda_a\lambda_b\to\lambda_1\lambda_2\lambda_3} \cong\, & \delta_{\lambda_2\lambda_b}\mathcal{M}_{\gamma p\to\gamma p}(s_{23},t_2)\frac{eF_1(t_1)}{t_1}(p_a+p_1)^{\mu} \\ & \times \varepsilon^*_{\mu}(p_3,\lambda_3)\delta_{\lambda_1\lambda_a} + \delta_{\lambda_1\lambda_a}\mathcal{M}_{\gamma p\to\gamma p}(s_{13},t_1) \\ & \times \frac{eF_1(t_2)}{t_2}(p_b+p_2)^{\mu}\varepsilon^*_{\mu}(p_3,\lambda_3)\delta_{\lambda_2\lambda_b}.\end{aligned} \tag{2.21}$$

Using $\vec{q}_{1,2\perp} = -\vec{p}_{1,2\perp}$ we then have

$$\begin{aligned}\mathcal{M}_{\lambda_a\lambda_b\to\lambda_1\lambda_2\lambda_3} \cong\, & \delta_{\lambda_2\lambda_b}\mathcal{M}_{\gamma p\to\gamma p}(s_{23},t_2)\frac{eF_1(t_1)}{t_1}\frac{2}{z_1} \\ & \times \frac{V^*(q_{1\perp},\lambda_3)}{\sqrt{1-z_1}}\delta_{\lambda_1\lambda_a} \\ & + \delta_{\lambda_1\lambda_a}\mathcal{M}_{\gamma p\to\gamma p}(s_{13},t_1)\frac{eF_1(t_2)}{t_2}\frac{2}{z_2} \\ & \times \frac{V^*(q_{2\perp},\lambda_3)}{\sqrt{1-z_2}}\delta_{\lambda_2\lambda_b},\end{aligned} \tag{2.22}$$

where the longitudinal momentum fractions of outgoing protons $z_{1,2}$ are

$$z_1 \cong \frac{s_{23}}{s}, \qquad z_2 \cong \frac{s_{13}}{s}, \qquad z_1, z_2 < 1, \tag{2.23}$$

and $V(q_\perp, \lambda_3)$ can be calculated from the x, y components of the momenta of participating protons (see Ref. [27]),

$$V(q_\perp, \lambda_3 = \pm 1) = \mathbf{e}^{(\lambda_3)}_{\mu} q^{\mu}_{\perp} = -\frac{1}{\sqrt{2}}(\lambda_3 q_x + i q_y). \tag{2.24}$$

E. Equivalent-photon approximation

The cross section for the $\gamma\pi^0$ exchange and $\gamma\mathbb{P}$ exchange mechanisms can also be calculated in the equivalent-photon approximation. In this approach the distribution of the photon can be written as

$$\begin{aligned}\frac{d\sigma}{dy dp^2_\perp} =\, & z_1 f(z_1)\frac{d\sigma_{\gamma p\to\gamma p}}{dt_2}(s_{23}, t_2 \approx -p^2_\perp) \\ & + z_2 f(z_2)\frac{d\sigma_{\gamma p\to\gamma p}}{dt_1}(s_{13}, t_1 \approx -p^2_\perp),\end{aligned} \tag{2.25}$$

where $f(z)$ is a photon flux in the proton; an explicit formula can be found, e.g., in Ref. [29]. The differential distribution of elastic scattering at high energies is parametrized as

$$\frac{d\sigma_{\gamma p\to\gamma p}}{dt}(s,t) = \frac{|\mathcal{M}_{\gamma p\to\gamma p}(s,t)|^2}{16\pi s^2}. \tag{2.26}$$

First the energy and longitudinal momentum of the photon are calculated as a function of photon rapidity and transverse momentum $p_\perp = \sqrt{p^2_x + p^2_y}$,

$$E_\gamma = p_\perp \cosh y, \qquad p_z = p_\perp \sinh y. \tag{2.27}$$

We get

$$\begin{aligned} & p_z = \sqrt{E^2_\gamma - p^2_\perp} \quad \text{for } y > 0 \quad \text{and} \\ & p_z = -\sqrt{E^2_\gamma - p^2_\perp} \quad \text{for } y < 0.\end{aligned} \tag{2.28}$$

Then energies in the photon-proton subsystems can be calculated approximately as

$$\begin{aligned} & s_{13} \approx (p_{a0} + E_\gamma)^2 - (p_{az} + p_z)^2, \\ & s_{23} \approx (p_{b0} + E_\gamma)^2 - (p_{bz} + p_z)^2.\end{aligned} \tag{2.29}$$

The fractional energy losses of the protons (z_1 and z_2) with four-momenta p_a and p_b, respectively, can be obtained from Eq. (2.23).

III. RESULTS

In the following section we shall show the results of the differential distributions for the exclusive bremsstrahlung mechanisms discussed in the previous section. The amplitudes for processes discussed in the sections above are calculated numerically for each point in the phase space. In calculating the cross section of the three-body process we perform integrations in $\xi_1 = \log_{10}(p_{1\perp}/1\ \text{GeV})$ and $\xi_2 = \log_{10}(p_{2\perp}/1\ \text{GeV})$—instead of in $p_{1\perp}$ and $p_{2\perp}$—in the photon (pseudo) rapidity η_γ and the relative azimuthal angle between the outgoing protons $\phi_{12} = \phi_1 - \phi_2$.

The photon energy spectrum drops relatively slowly with photon energy, as is shown in Fig. 5 (left panel). The ZDC detectors (at ATLAS or CMS) can measure only photons above some energy threshold (e.g., $E_\gamma >$ 50 GeV). In the calculation of classical bremsstrahlung

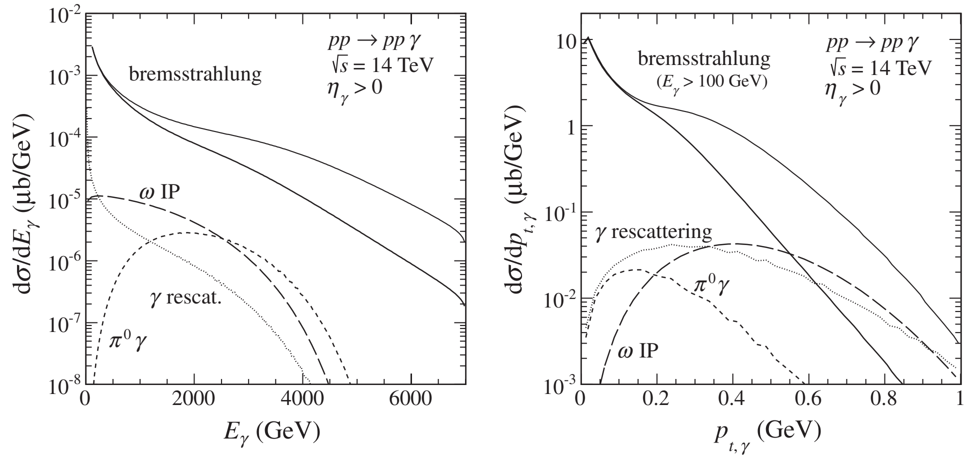

FIG. 5. Energy spectrum of photons (left panel) and distribution in transverse momentum of photons (right panel) for all processes considered here at $\sqrt{s} = 14$ TeV and for $\eta_\gamma > 0$. For classical bremsstrahlung we have imposed $E_\gamma > 100$ GeV and used two values of $\Lambda_N = 0.8$, 1 GeV in the proton off-shell form factors [Eq. (2.9)] (see the lower and upper solid line, respectively).

presented here we assume $E_\gamma > 100$ GeV as an example. Corresponding distributions in the photon transverse momentum are shown in Fig. 5 (right panel). The contribution of classical bremsstrahlung is concentrated at very small transverse momenta, which is consistent with a very small photon emission angle (large pseudorapidity). The other distributions have rather similar shapes and vanish at $p_{\perp,\gamma} = 0$ GeV. The exact shape may depend somewhat on the functional form and values of the cutoff parameters of off-shell form factors taking into account the non-pointlike nature of the vertices involved. Here we have fixed the values of the corresponding form factors at typical hadronic scales.

In Fig. 6 we show an auxiliary distribution in $\xi_1 = \log_{10}(p_{1\perp}/1\ \text{GeV})$ (left panel) and $\xi_2 = \log_{10}(p_{2\perp}/1\ \text{GeV})$ (right panel), where $p_{1\perp}$ and $p_{2\perp}$ are outgoing proton transverse momenta. For example, $\xi = -1$ means a proton transverse momenta of 0.1 GeV. The biggest contribution for the classical bremsstrahlung process comes from the region $\xi_i \approx -0.5$ (i.e., $p_{i\perp} \approx 0.3$ GeV). The distributions in ξ_1 or ξ_2 are different because we have limited to the case of $\eta_\gamma > 0$ only.

In Fig. 7 we show corresponding two-dimensional distributions in (ξ_1, ξ_2) in a full range of photon (pseudo) rapidity. A quite different pattern can be seen for different mechanisms. For the classical bremsstrahlung we observe an enhancement along the diagonal. This enhancement is a reminiscence of the elastic scattering for which $\xi_1 = \xi_2$. Photon rescattering on the pion cloud (panel c) and photon rescattering with pomeron exchange (panel d) are concentrated at small ξ_1 or ξ_2.

The photon (pseudo)rapidity distribution is particularly interesting. In Fig. 8 we show both the distribution for photons η_γ (left panel) and corresponding distribution

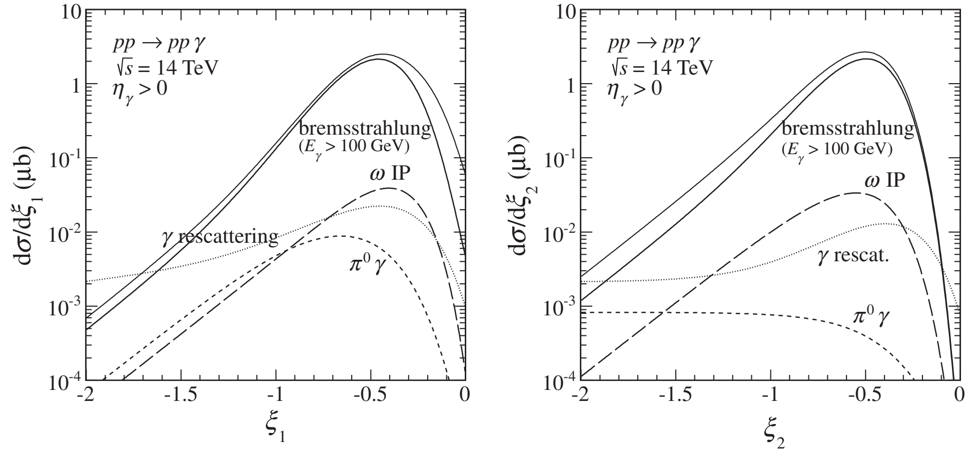

FIG. 6. Distribution in $\xi_1 = \log_{10}(p_{1\perp}/1\ \text{GeV})$ (left panel) and $\xi_2 = \log_{10}(p_{2\perp}/1\ \text{GeV})$ (right panel) at $\sqrt{s} = 14$ TeV and for $\eta_\gamma > 0$. For classical bremsstrahlung $E_\gamma > 100$ GeV and we have used two values of $\Lambda_N = 0.8$, 1 GeV (see the lower and upper solid line, respectively).

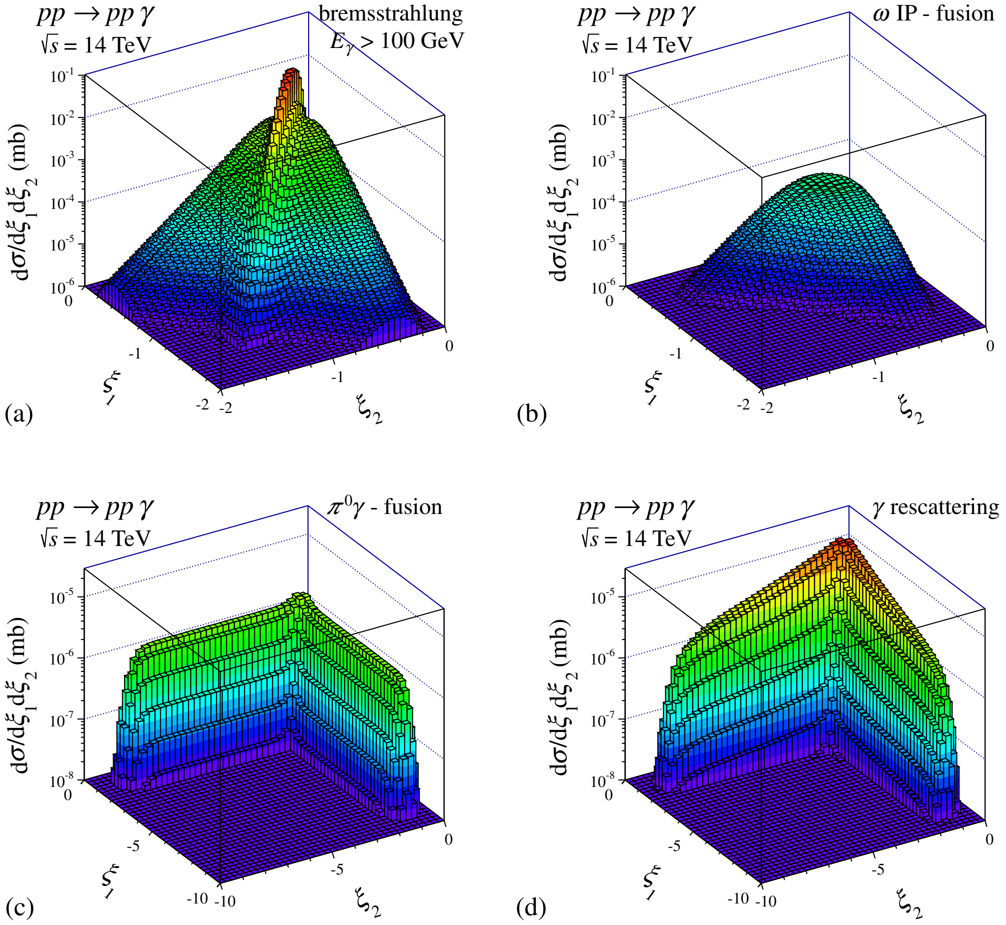

FIG. 7 (color online). Distribution in $(\xi_1, \xi_2) = (\log_{10}(p_{1\perp}/1\mathrm{GeV}), \log_{10}(p_{2\perp}/1\ \mathrm{GeV}))$ for the classical bremsstrahlung (a), the ω-rescattering (b), the pion-cloud (c), and the γ-rescattering (d) mechanisms at $\sqrt{s} = 14$ TeV. In addition, for the classical bremsstrahlung we have imposed $E_\gamma > 100$ GeV and used $\Lambda_N = 1$ GeV in the proton off-shell form factors.

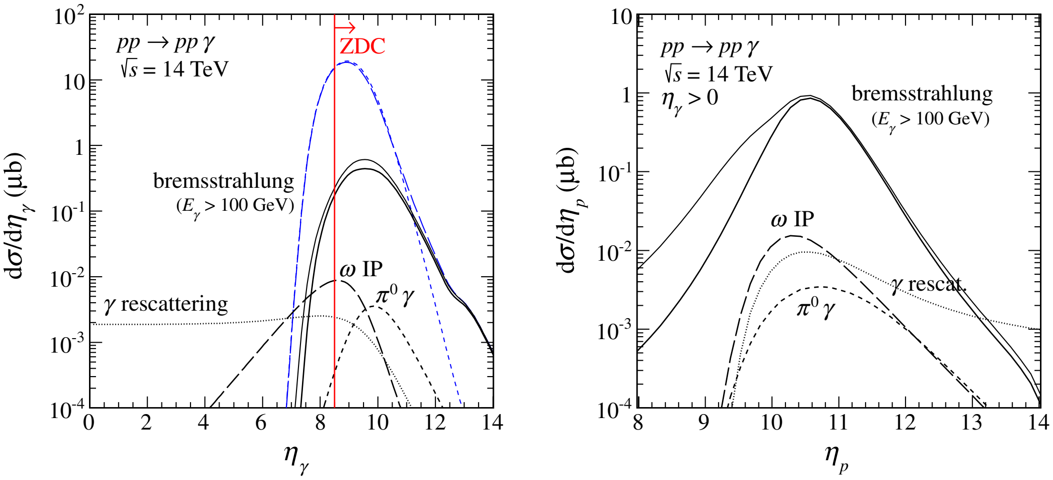

FIG. 8 (color online). Distribution in (pseudo)rapidity of emitted photons (left panel) and in pseudorapidity of outgoing protons (right panel) at $\sqrt{s} = 14$ TeV. For classical bremsstrahlung we have imposed $E_\gamma > 100$ GeV and used two values of $\Lambda_N = 0.8$, 1 GeV (see the lower and upper solid line, respectively). A large cancellation between the initial- (2.3) and final-state radiation (2.1) is shown (see the blue short-dashed and the blue long-dashed lines, respectively). The lower-pseudorapidity limit for the CMS ZDC detector ($\eta_\gamma > 8.5$) is shown by the vertical line.

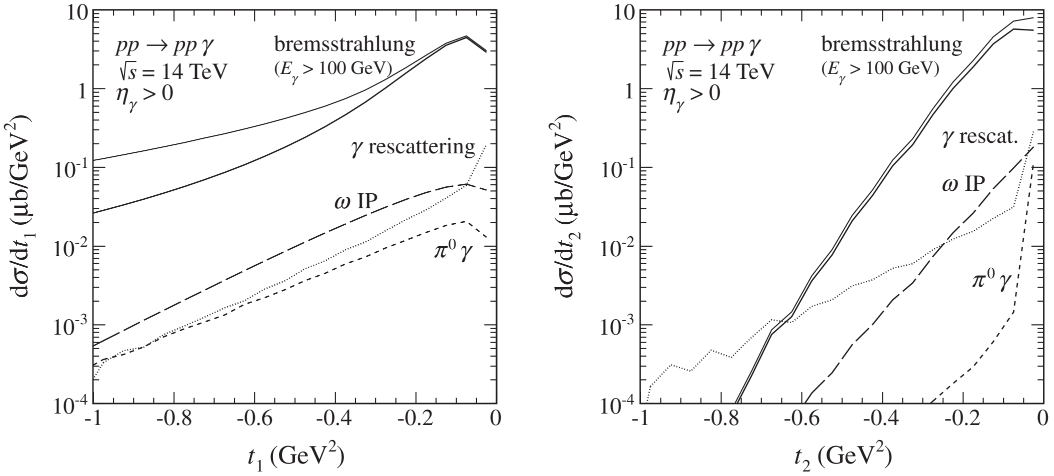

FIG. 9. Distribution in four-momentum squared t_1 (left panel) and t_2 (right panel) at $\sqrt{s} = 14$ TeV and for $\eta_\gamma > 0$. For classical bremsstrahlung we have imposed $E_\gamma > 100$ GeV and used two values of $\Lambda_N = 0.8$, 1 GeV (see the lower and upper solid line, respectively).

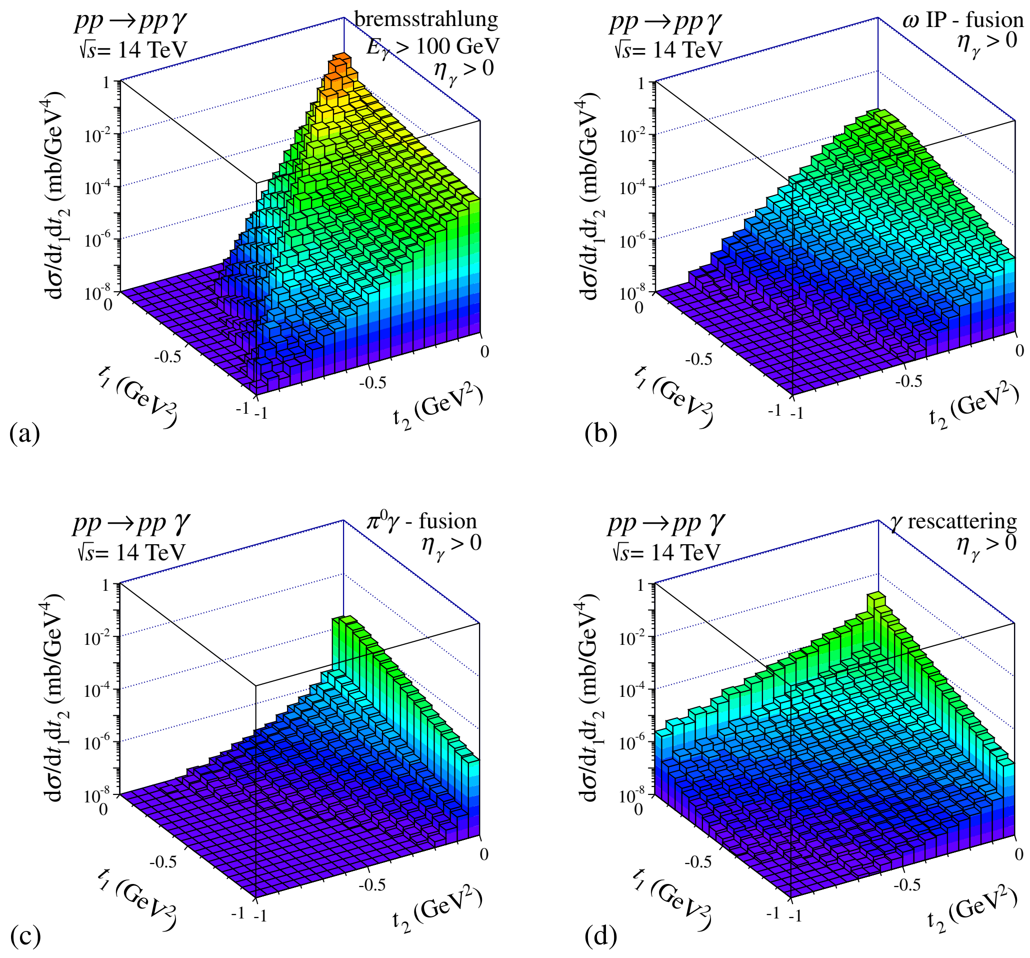

FIG. 10 (color online). Distribution in (t_1, t_2) for the classical bremsstrahlung (a) ($E_\gamma > 100$ GeV and $\Lambda_N = 1$ GeV), the ω-rescattering (b), the pion-cloud (c), and the γ-rescattering (d) contributions at $\sqrt{s} = 14$ TeV and for $\eta_\gamma > 0$.

for outgoing protons η_p (right panel) for all processes considered in the present paper. In this variable both protons and photons are localized in a similar region of pseudorapidities (or equivalently polar angles). The classical bremsstrahlung clearly gives the largest contribution. It is also concentrated at very large η_γ, i.e., in the region where ZDC detectors can be used. We observe a large cancellation between the corresponding terms in the amplitudes (2.1) and (2.3) (see left panel) or (2.2) and (2.4). The γ-rescattering process with pomeron exchange clearly dominates in the region of $\eta_\gamma < 6$. The cross section for this process is rather small. Clearly an experimental measurement there would be a challenge.

In a first experimental trial one could measure only photons and perform a check for a rapidity gap in the midrapidity region. If protons are measured as well, one could analyze also some new observables related to protons. In Fig. 9 we show the distribution in the four-momentum transfer squared between initial and final protons. One can observe a change of slope of the t distribution, which is caused by the bremsstrahlung of photons. In our simplified model we have assumed a constant (in t_1 and t_2) energy-dependent slope.

In Fig. 10 we show the distribution in two-dimensional space (t_1, t_2). For the classical bremsstrahlung (left panel) one can observe a ridge when $t_1 \simeq t_2$, which is a reminiscence of elastic scattering. The distributions discussed here could in principle be obtained with the TOTEM detector at CMS to supplement the ZDC detector for the measurement of photons.

In Fig. 11 we compare the distribution in the photon (forward proton) subsystem energy for all processes considered in the present paper. The $pp \to pp\gamma$ process discussed here gives a sizeable contribution to the low-mass ($M_X > m_p$) single diffractive cross section.

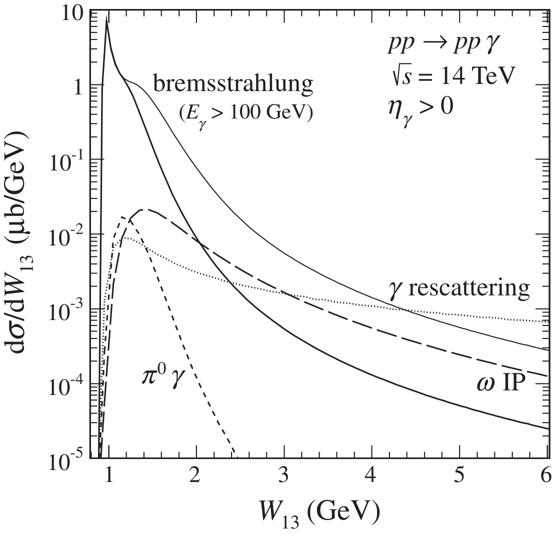

FIG. 11. Distribution in the γp subsystem energy W_{13} for all processes considered here at $\sqrt{s} = 14$ TeV and for $\eta_\gamma > 0$. For classical bremsstrahlung we have imposed $E_\gamma > 100$ GeV and used two values of $\Lambda_N = 0.8$, 1 GeV (see the lower and upper solid line, respectively).

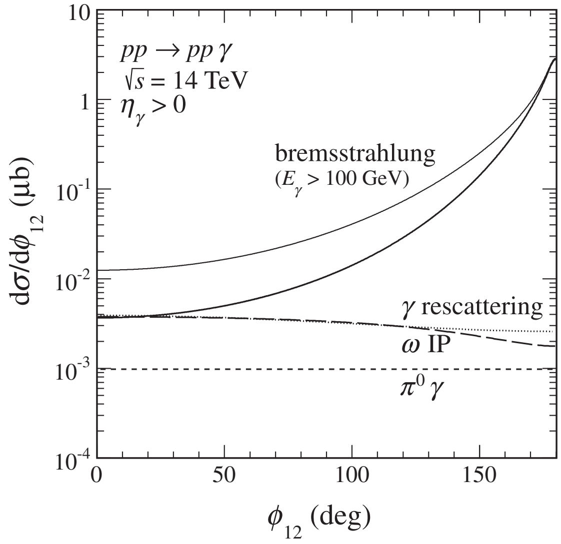

FIG. 12. Distribution in relative azimuthal angle between outgoing protons for different mechanisms at $\sqrt{s} = 14$ TeV and for $\eta_\gamma > 0$. For classical bremsstrahlung we have imposed $E_\gamma > 100$ GeV and used two values of $\Lambda_N = 0.8$, 1 GeV (see the lower and upper solid line, respectively).

If both protons are measured one could also study correlations in the relative azimuthal angle between outgoing protons. Our model calculations are shown in Fig. 12. One can observe a large enhancement at back-to-back configurations for the classical bremsstrahlung, which recalls the elastic-scattering case ($\phi_{12} = \pi$). The contributions for other mechanisms are significantly smaller and weakly depend on ϕ_{12}.

IV. CONCLUSIONS

In this paper we have considered several mechanisms of exclusive single-photon production. We have calculated several differential distributions for the $pp \to pp\gamma$ reaction at high energy for the first time in the literature. The classical bremsstrahlung mechanism turned out to give the biggest cross section concentrated at large photon (pseudo) rapidities. The photons are emitted at only slightly smaller pseudorapidities than the scattered protons. We observe a strong cancellation between the initial- and final-state radiation. The cross section for the classical bremsstrahlung is peaked at back-to-back configurations (similar transverse momenta or polar angles of outgoing protons and relative azimuthal angle concentrated close to $\phi_{12} = \pi$). This is a clear reminiscence of elastic scattering. The cut on photon energy ($E_\gamma > 100$ GeV) reduces the region of $\phi_{12} \cong \pi$ significantly and the integrated diffractive bremsstrahlung cross section is only of the order of μb. The cross section for pion-photon or photon-pion exchanges is much smaller. Here both small (photon exchange) and large (pion exchange) four-momentum transfers squared are possible. For this process there is no correlation in azimuthal angle between outgoing protons.

Both the classical bremsstrahlung and the pion-photon (photon-pion) fusion as well as the virtual-ω–rescattering mechanisms could be studied with the help of the Zero Degree Calorimeters (photons) and the ALFA or TOTEM detectors (protons). By imposing several cuts one could select or enhance the contribution of one of the mechanisms. The cross section for pomeron-photon or photon-pomeron exchanges is rather small and concentrated at midrapidities. Furthermore, the transverse momenta of outgoing photons are small and cannot be easily measured with central ATLAS or CMS detectors.

Summarizing, even present LHC equipment allows one to study the exclusive production of photons. Since this process was never studied at high energies it is worth making efforts to obtain first experimental cross sections. Since the cross sections are reasonably large one could try to obtain even some differential distributions. This would allow one to test our understanding of the diffractive processes and help in pinning down some hadronic and electromagnetic off-shell form factors, which are otherwise difficult to test.

ACKNOWLEDGMENTS

We are indebted to W. Schäfer for a discussion of some theoretical aspects of our calculation and J. Lämsä, M. Murray, and R. Orava for a discussion of some experimental aspects. This work was partially supported by the Polish grant No. PRO-2011/01/N/ST2/04116.

[1] K. Nakayama and H. Haberzettl, Phys. Rev. C **80**, 051001 (2009); K. Nakayama and F. Huang, Phys. Rev. C **82**, 065201 (2010); A. Johansson, H. Haberzettl, K. Nakayama, and C. Wilkin, Phys. Rev. C **83**, 054001 (2011).

[2] S. Kondratyuk, G. Martinus, and O. Scholten, Phys. Lett. B **418**, 20 (1998); M. D. Cozma, G. H. Martinus, O. Scholten, R. G. E. Timmermans, and J. A. Tjon, Phys. Rev. C **65**, 024001 (2002).

[3] A. Cisek, P. Lebiedowicz, W. Schäfer, and A. Szczurek, Phys. Rev. D **83**, 114004 (2011).

[4] P. Lebiedowicz and A. Szczurek, Phys. Rev. D **87**, 074037 (2013).

[5] S. D. Drell and K. Hiida, Phys. Rev. Lett. **7**, 199 (1961); R. T. Deck, Phys. Rev. Lett. **13**, 169 (1964).

[6] G. Alberi and G. Goggi, Phys. Rep. **74**, 1 (1981).

[7] V. A. Khoze, J. W. Lämsä, R. Orava, and M. G. Ryskin, JINST **6**, P01005 (2011); H. Grönqvist, V. A. Khoze, J. W. Lämsä, M. Murray, and R. Orava, arXiv:1011.6141.

[8] O. A. Grachov *et al.* (CMS Collaboration), J. Phys. Conf. Ser. **160**, 012059 (2009).

[9] P. Jenni, M. Nessi, and M. Nordberg (ATLAS Collaboration), Report Nos. LHCC-I-016, CERN-LHCC-2007-001.

[10] P. Lebiedowicz and A. Szczurek, Phys. Rev. D **83**, 076002 (2011).

[11] M. G. Albrow, A. De Roeck, V. A. Khoze, J. Lämsä, E. Norbeck, Y. Onel, R. Orava, A. Penzo, and M. G. Ryskin, J. Instrum. **4**, P10001 (2009).

[12] J. Beringer *et al.* (Particle Data Group), Phys. Rev. D **86**, 010001 (2012).

[13] A. Donnachie and P. V. Landshoff, Phys. Lett. B **296**, 227 (1992).

[14] Y. Oh, A. I. Titov, and T.-S. H. Lee, Phys. Rev. C **63**, 025201 (2001).

[15] M. Diehl, Eur. Phys. J. C **6**, 503 (1999).

[16] H. Haberzettl and K. Nakayama, Phys. Rev. C **85**, 064001 (2012).

[17] O. Nachtmann, in Exclusive and diffractive processes in high energy proton-proton and nucleus-nucleus collisions, Trento, Italy, 2012 (unpublished).

[18] C. Ewerz, M. Maniatis, and O. Nachtmann (in preparation).

[19] P. Lebiedowicz, O. Nachtmann, and A. Szczurek (in preparation).

[20] P. Lebiedowicz and A. Szczurek, Phys. Rev. D **81**, 036003 (2010); P. Lebiedowicz, R. Pasechnik, and A. Szczurek, Phys. Lett. B **701**, 434 (2011); P. Lebiedowicz and A. Szczurek, Phys. Rev. D **85**, 014026 (2012).

[21] R. Machleidt, K. Holinde, and C. Elster, Phys. Rep. **149**, 1 (1987); R. Machleidt, Adv. Nucl. Phys. **19**, 189 (1989).

[22] N. Kaiser, Phys. Rev. C **60**, 057001 (1999).

[23] K. Nakayama, Y. Oh, J. Haidenbauer, and T.-S. H. Lee, Phys. Lett. B **648**, 351 (2007).

[24] A. Szczurek and V. Uleshchenko, Eur. Phys. J. C **12**, 663 (2000).

[25] H. Holtmann, A. Szczurek, and J. Speth, Nucl. Phys. **A596**, 631 (1996).

[26] T. E. O. Ericson, B. Loiseau, and A. W. Thomas, Phys. Rev. C **66**, 055206 (2002).

[27] W. Schäfer and A. Szczurek, Phys. Rev. D **76**, 094014 (2007).

[28] S. Donnachie, G. Dosch, P. Landshoff, and O. Nachtmann, *Pomeron physics and QCD* (Cambridge University Press, Cambridge, England, 2002).

[29] M. Drees and D. Zeppenfeld, Phys. Rev. D **39**, 2536 (1989).